Three-Dimensional Folding of the tRNA-like Domain of *Escherichia coli* tmRNA†

Christian Zwieb,‡ Sadel A. Guven,§ Iwona K. Wower,§ and Jacek Wower*,§

Department of Molecular Biology, The University of Texas Health Science Center at Tyler, 11937 U.S. Highway 271, Tyler, Texas 75708-3154, and Department of Animal and Dairy Sciences, Program in Cell and Molecular Biosciences, Auburn University, 210 Upchurch Hall, Auburn, Alabama 36849-5415

Received March 5, 2001; Revised Manuscript Received June 12, 2001

ABSTRACT: UV irradiation of *Escherichia coli* tmRNA both on and off the ribosome induced covalent cross-links between its 3′- and its 5′-terminal segments. Cross-linking was unaffected in a molecule that lacked the tag-peptide codon region and pseudoknots 2, 3, and 4. Intact and truncated cross-linked tmRNAs were aminoacylated as efficiently as the respective nonirradiated molecules, suggesting that the added UV-induced bonds did not disturb tmRNA conformation. Using RNase H digestion followed by primer extension with reverse transcriptase, two cross-linked sites were identified within the tRNA-like region of tmRNA. The first was formed between nucleotides U9/U10 near the 5′ end and nucleotides C346/U347 in the T loop. The second cross-link involved residues at positions 25−28 and 326−329 within helix 2a. Together with comparative sequence analysis, these findings yielded a three-dimensional model of the tRNA-like domain of *E. coli* tmRNA. Despite significant reduction of the D domain and the proximity of U9/U10 and C346/U347, the model closely resembles the L-shaped structure of canonical tRNA.

Transfer-messenger RNA (tmRNA), previously known as 10Sa RNA or SsrA RNA, is an essential component of trans-translation, a process that rescues ribosomes stalled at the 3′ end of mRNAs lacking the stop codon. Incompletely synthesized proteins are tagged with a short peptide that is readily recognized by housekeeping proteases. tmRNA-like sequences have been identified in all bacteria and plastid and mitochondrial genomes (*1*, *2*). Evidence derived from comparative sequence analyses and in vitro probing of *Escherichia coli* tmRNA indicates that the molecule is composed of a tRNA- and an mRNA-like domain joined together by pseudoknots (*3*−*5*).

Current models of trans-translation suggest that aminoacylated tmRNA binds to the A site of the stalled ribosome, accepts the incomplete polypeptide from the P site-bound tRNA, and after translocation makes its mRNA-like domain available for decoding by incoming aminoacyl-tRNAs (*6*). To enter this process, tmRNA must have an intact 3′ CCA terminus and be aminoacylated. Repair of the 3′ CCA sequence is facilitated by ATP/CTP tRNA nucleotidyl transferase (*7*). In *E. coli* and *Bacillus subtilis*, aminoacylation is catalyzed by alanyl-tRNA synthetase (*8*, *9*). Binding of Ala-tmRNA[1] to ribosomes is assisted by the elongation factor Tu (EF-Tu) and protein SmpB and depends on ribosomal protein S1 (*7*, *10*, *11*).

Although these findings provide insight into the first stage of trans-translation, numerous questions remain unanswered. To what extent is the three-dimensional folding of the tRNA-like domain of tmRNA different from the structure of canonical tRNA? Are the peculiar features of the tRNA-like domain important for tmRNA function and required for recognition by proteins? Does tmRNA have an analogue of the anticodon arm, which is essential for binding canonical tRNA to ribosomes and translocation? A detailed understanding of the mechanism of trans-translocation is dependent on the three-dimensional structure of the tRNA-like domain and how folding might be affected after binding of tmRNA to the ribosome.

Irradiation of RNA molecules with far-UV light (∼254 nm) has been a valuable method for defining three-dimensional constraints in the folding of *E. coli* $tRNA^{Phe}$ (*12*), *Tetrahymena* ribozyme (*13*), and 16S and 23S ribosomal RNAs (*14*). We have used this approach to gain insight into the folding of the tRNA-like domain of *E. coli* tmRNA. Regardless of whether it is bound to ribosomes or it is free in solution, two sets of UV cross-links were introduced into the tRNA-like domain of *E. coli* tmRNA. Although tmRNA was synthesized by transcription in vitro and thus contained unmodified nucleotides, cross-linked tmRNA could be aminoacylated efficiently to demonstrate that cross-links were present in properly folded RNA. When combined with results obtained by comparative sequence analysis of 79 representative tmRNA sequences, the cross-linking data yielded a high-resolution three-dimensional model of the tRNA-like domain of tmRNA.

MATERIALS AND METHODS

Chemicals and Enzymes. Nucleotides, deoxyribonucleotides, dideoxynucleotides, and T4 RNA ligase were obtained from Pharmacia. ATP/CTP tRNA nucleotidyl transferase was

† This work was supported by National Institute of Health Grant GM58267 to J.W. Publication costs were supported in part by the Upchurch Fund for Excellence in Animal and Dairy Sciences.

* To whom correspondence should be addressed. Tel: (334) 844-1508; fax: (334) 844-1519; e-mail: jwower@acesag.auburn.edu.

‡ The University of Texas Health Science Center at Tyler.

§ Auburn University.

[1] Abbreviations: Ala-tmRNA, alanyl-tmRNA; EF-Tu, elongation factor Tu; ssrA, small stable RNA A; tmRNAΔ90−299, truncated tmRNA derivative lacking nucleotides 90−299; XL-tmRNA and tmRNAΔ90−299, internally cross-linked tmRNA derivatives.

10.1021/bi010443v CCC: $20.00
Published on Web 07/18/2001

isolated from yeast as described by Sternbach et al. (*15*). T7 RNA polymerase was from U.S. Biochemical Corp. AMV reverse transcriptase was from Life Sciences, Inc. RNase H was acquired from Takara Biomedicals. Phage T4 polynucleotide kinase (3′ phosphatase-free) was purchased from Boehringer Mannheim Corp. Restriction enzyme *Bst*NI was from New England Biolabs. All radiochemicals were purchased from ICN Biochemicals, Inc.

Synthesis and Purification of tmRNA Derivatives. E. coli tmRNA and its truncated derivative tmRNAΔ90−299 were synthesized by runoff transcription of *Bst*NI-linearized plasmids (ptmR and ptmΔ90−299) with T7 RNA polymerase. Construction of plasmids, transcription conditions, and purification of tmRNA transcripts were as described previously (*7*).

Purified tmRNA transcripts, approximately 6% of which lacked a 3′ terminal adenosine, were ^{32}P-labeled at their 3′ ends with yeast ATP/CTP tRNA nucleotidyl transferase in the presence of [α-^{32}P]ATP (*7*). 5′-^{32}P-labeled tmRNAs were obtained by dephosphorylating with calf intestinal phosphatase and phosphorylating with crude [γ-^{32}P]ATP and T4 polynucleotide kinase. ^{32}P-labeled tmRNAs were repurified on 6% polyacrylamide gels (40:1) in native TGE buffer (25 mM Tris, 190 mM glycine, 1 mM EDTA, and 2.5% glycerol). The integrity of the transcripts was confirmed by electrophoresis on a denaturing 6% polyacrylamide gel (acrylamide:*N*,*N*′-methylenebisacrylamide = 19:1) in 100 mM Tris/100 mM H_3BO_4 (pH 8.3) containing 2.5 mM EDTA and 8 M urea.

Aminoacylation. Gel-purified 3′-^{32}P-labeled tmRNA, tmRNAΔ90−299, and their cross-linked derivatives (XL-tmRNA and XL-tmRNAΔ90−299) were incubated for 30 min at 37 °C, aminoacylated according to Sampson and Uhlenbeck (*16*), and analyzed by gel-shift electrophoresis as described by Varshney et al. (*17*). Prior to electrophoresis, Ala-tmRNA was digested with RNase T_1 in 10 mM sodium acetate (pH 4.5) to yield aminoacylated 3′-terminal octamer, CUCCACCA-Ala.

Cross-Linking of tmRNA. Gel-purified ^{32}P-labeled tmRNA derivatives were resuspended in 10 mM Tris-HCl (pH 7.6), 10−15 mM $MgCl_2$, and 25 mM KCl and incubated for 30 min at 37 °C. Cross-linking was accomplished by irradiating 1 μM [^{32}P]tmRNA at 0 °C in a Rayonet model RPR-100 photochemical reactor equipped with four RPR-2540-Å lamps as described by Wower et al. (*18*). Ten microliter aliquots were removed at the times indicated in the Results section, and the products were analyzed on denaturing 8% polyacrylamide gels. The cross-linking yield was determined using Phosphoimager SI and ImageQuant 1.2 software from Molecular Dynamics. Cross-linking and purification of tmRNA complexes with *E. coli* ribosomal protein S1 and 70S ribosomes were carried out as described previously (*7*).

Analysis of Cross-Linked tmRNA. Sites of cross-linking were determined by digestion of purified cross-linked tmRNAs with RNase H in the presence of chosen oligodeoxyribonucleotides (*19*) in combination with primer extension using reverse transcriptase (*20*). Oligodeoxyribonucleotides a−g were complementary to the following regions (*E. coli* tmRNA numbering): 335−348 (a), 325−339 (b), 317−329 (c), 304−318 (d), 256−270 (e), 31−45 (f), and 3−15 (g). To generate precise cleavages in the D and T regions of tmRNA, RNase H digestions were carried out using chimeric oligonucleotides h1−h3, consisting of four deoxynucleotide residues connected (in the 5′- to 3′-direction) to a stretch of 9−15 2′-*O*-methylribonucleotides and a ribocytidine residue (*21*). Deoxy(TGAA)-2′-OMe-(CCCGCGUCCGAAAUU)-riboC (h1), deoxy(CCGC)-2′-OMe-(GUCCGAAAUU)-riboC (h2), and deoxy(TCCA)-2′OMe-(GAATCAGCC)-riboC (h3) were complementary to nucleotides at positions 327−345, 325−339, and 2−15, respectively. Primer extension analysis of the T arm was carried out with a dodecadeoxyribonucleotide (3′-oligo) complementary to the 3′ end of tmRNA (residues 352−363). The 5′ end of tmRNA was scanned using a pentadecamer (5′-oligo) complementary to nucleotides 53−67.

Comparative Sequence Analysis of tmRNA. The tmRNA alignment, obtained from the tmRNA database tmRDB at the URL http:psyche.uthct.edu/dbs/tmRDB/tmRDB.html (*22*), was updated for a total of 79 representative tmRNA sequences. Abbreviated species names (ordered phylogenetically) using tmRDB identifications were as follows: AQU.AEO., THE.MAR., THE.THE., DEI.RAD., POR.GIN., CHL.TEP., CHL.TRA., CHL.PNE., CHL.PSI., ANA.SPE., NOS.PUN., SYN.SP-B, SYN.SP-A, ODO.SIN., POR.PUR., GUI.THE., THA.WEI., CYN.PAR., REC.AME., BOR.BUR., TRE.PAL., CAU.CRE., BRA.JAP., RHO.PAL., SIN.MEL., RIC.PRO., MET.EXT., NEI.GON., NIT.EUR., ALC.EUT., BOR.PER., DIC.NOD., FRA.TUL., XYL.FAS., LEG.PNE., ACI.FER., PSE.AER., PSE.PUT., THI.FER., SHE.PUT., ALT.HAL., MAR.HYD., PSE.HAL., VIB.CHO., AER.SAL., ESC.COL., KLE.PNE., SAL.PAR., YER.PES., ACT.ACT., HAE.INF., PAS.MUL., DES.DES., DES.VUL., GEO.SUL., HEL.PYL., CAM.JEJ., FUS.NUC., MYC.AVI., MYC.LEP., COR.DIP., STR.COE., BAC.MEG., BAC.SUB., BAC.ANT., STA.AUR., STA.EPI., ENT.FA-A, ENT.FA-B, STR.PYO., STR.GOR., STR.EQU., STR.MUT., STR.PNE., URE.URE., MYC.CAP., MYC.GEN., MYC.PNE., and CLO.DIF. The rules described previously determined Watson−Crick and G−U base pairs supported by comparative sequence analysis (*5*, *23*). The degree of conservation was measured by visual inspection of the alignment.

tmRNA Modeling. The tRNA-like domain of *E. coli* tmRNA was modeled with the program ERNA-3D (*24*; URL http://www.molgen.mpg.de/~ag_ribo/ag_brimacombe/ERNA3D/ERNA-3D.html) on a SiliconGraphics Octane workstation. PDB coordinates for modeling of selected tmRNA regions were extracted from yeast $tRNA^{Phe}$ (*25*, accession number 6TNA) and 23S rRNA (*26*, 1FFK), available at the Protein Data Bank at http://www.rcsb.org/pdb/. The RNA hammerhead ribozyme coordinates (*27*, ID code urx057) were from the Nucleic Acid Database Project (http://ndbserver.rutgers.edu/NDB/). The model was refined using VCMD software (*28*).

RESULTS

UV Cross-Linking of Unmodified E. coli tmRNA on and off 70S Ribosomes. Irradiation of tmRNA-70S ribosome−ribosomal protein S1 complexes (*7*) and free unmodified tmRNA with 254 nm light yielded internally cross-linked tmRNA species (XL-tmRNA) displaying the same slow mobilities on denaturing polyacrylamide gels (Figure 1A, lanes 1 and 3). XL-tmRNAs were formed at an initial rate of 0.05 min^{-1} and accumulated for about 20 min (Figure

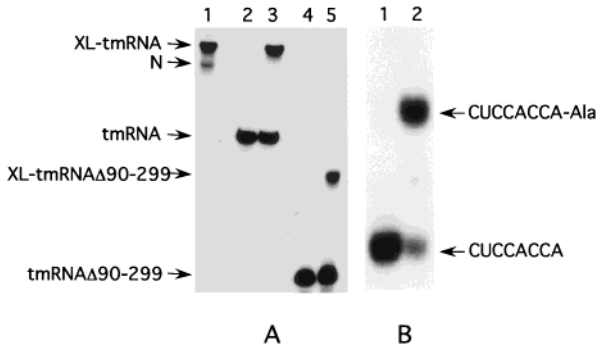

FIGURE 1: UV cross-linking of the *E. coli* tmRNA^{Ala} and its aminoacylation. Panel A: Analysis of 3′-^{32}P-labeled internally cross-linked tmRNA derivatives (XL-tmRNA) on a denaturing 8% polyacrylamide gel. Lane 1, XL-tmRNA isolated from UV-irradiated tmRNA-70S ribosome complexes and digested with proteinase K. Lane 2, nonirradiated tmRNA (control). Lane 3, XL-tmRNA formed after UV irradiation of free tmRNA. Lane 4, nonirradiated tmRNAΔ90−299 (control). Lane 5, XL-tmRNAΔ90−299 formed after UV irradiation of tmRNAΔ90−299. N is a product of degradation formed during proteinase K digestion of the covalent tmRNA−ribosomal protein S1 complexes. Panel B: Analysis of aminoacylation of 3′-^{32}P-labeled XL-tmRNA on a 15% polyacrylamide gel as described by Wower et al. (*7*). CUCCACCA (lane 1) and CUCCACCA-Ala (lane 2) formed after RNase T_1 digestion of nonaminoacylated XL-tmRNA and Ala-XL-tmRNA.

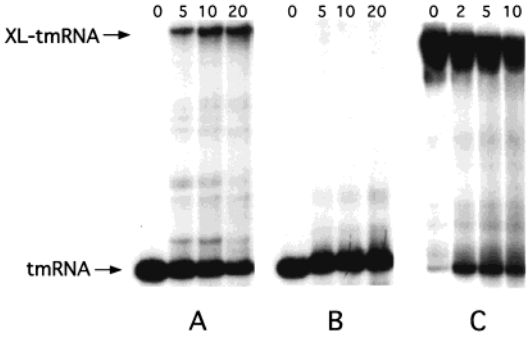

FIGURE 2: UV cross-linking of the *E. coli* tmRNA^{Ala}. Panel A: Time course of cross-linking of 3′-^{32}P-labeled tmRNA after its irradiation with UV light in 10 mM Tris-HCl (pH 7.6), 15 mM $MgCl_2$, and 25 mM KCl. Panel B: As panel A, except with 3.5 M urea and no $MgCl_2$. Panel C: UV-induced photoreversal of cross-links in a purified [3′-^{32}P]-XL-tmRNA. Analyses were carried out on denaturing 8% polyacrylamide gels. Numbers above lanes refer to minutes of irradiation.

2A). Typically, about 15% of the free tmRNA converted to XL-tmRNA derivative within that period. The intramolecular cross-link could be reversed after additional irradiation with short wavelength UV light (Figure 2C). The XL-tmRNA was not fluorescent and resisted a 15 min long treatment with 0.1 M HCl (not shown). No photoproducts were formed when tmRNA was irradiated in a low ionic strength buffer lacking magnesium ions and containing 3.5 M urea (Figure 2B), conditions that are known to disrupt the tertiary structure of tRNA (*12*).

Typically, 98% of the gel-purified 3′-^{32}P-labeled XL-tmRNA could be charged with alanine (Figure 1B). Such efficient aminoacylation indicated that neither the cross-link(s) nor the potential damage caused by UV irradiation significantly affected the three-dimensional folding of the tRNA-like domain of tmRNA. Digestion of both nonaminoacylated and aminoacylated XL-tmRNA with RNase T_1 released CUCCACCA and CUCCACCA-Ala, showing that the 3′-terminal octamer was not cross-linked.

Topography of Intra-Cross-Linking Sites. Substantial retardation of the XL-tmRNA on denaturing polyacrylamide gels (Figures 1A and 2A), attributed by earlier cross-linking studies to looped structures of cross-linked RNA (*12*, *13*), indicated that the cross-linked residues were located far apart. Two approaches were combined to identify the cross-linked residues. Oligodeoxyribonucleotide-directed cleavage of XL-tmRNA with RNase H was used to distinguish cross-linked segments from uncross-linked fragments (*19*). Cross-linked portions of XL-tmRNA were then scanned by primer extension (*20*).

The 3′-^{32}P-labeled XL-tmRNA was digested with RNase H and oligodeoxyribonucleotides placed strategically at increasing distances from the 3′ end. Such treatment yielded 3′-^{32}P-labeled tmRNA fragments of varying length. The location of the 3′-side segment of the cross-link was mapped by comparing differences in the digestion patterns between cross-linked and uncross-linked tmRNA. The mapping was repeated with 5′-^{32}P-labeled XL-tmRNA to reveal the 5′-side segment of the cross-link. These analyses indicated that cross-links were within the first and last 40 nucleotides of tmRNA (not shown), consistent with the presence of a large internal loop in XL-tmRNA and a significant retardation of cross-linked molecules on denaturing polyacrylamide gels (Figures 1A and 2A). Finally, RNase H, guided by oligodeoxyribonucleotide pairs, was used to excise segments of the internal loop region and isolate small cross-linked fragments.

An example of RNase H analysis of uncross-linked 3′-^{32}P-labeled tmRNA (control) and XL-tmRNA in the presence of five oligodeoxyribonucleotide pairs is shown in Figure 3C. Release of only one series of 3′-^{32}P-labeled fragments (diagonal D1) from tmRNA and two series of fragments (diagonals D2 and D3) from XL-tmRNA indicated that XL-tmRNA contained at least two cross-linked species. Because RNase H digestion of XL-tmRNA with oligodeoxyribonucleotides d and f produced only one 3′-^{32}P-labeled cross-linked piece, both cross-links were within the first and last 40 nucleotides. Release of two 3′-^{32}P-labeled fragments after digestion of XL-tmRNA with RNase H in the presence of pairs of oligodeoxyribonucleotides a/f and b/f delimited these two cross-linking sites to nucleotides 340−363 (x1) and 318−339 (x2) (Figure 3D). However, because RNase T_1 digestion of 3′-^{32}P-labeled XL-tmRNA released an octamer CUCCACCA (Figure 1B), cross-linking site x1 could be delimited even further to positions 340−355. An equivalent RNase H analysis of the 5′-^{32}P-labeled XL-tmRNA revealed two cross-linking sites within the first 40 5′-terminal residues (not shown).

Cross-linked nucleotides in the 3′- and 5′-terminal sequences of XL-tmRNA were identified by primer extension. This method relies on the ability of reverse transcriptase to arrest DNA synthesis at chemically modified, photodamaged, and cross-linked nucleotides (*29*−*31*). As shown in Figure 4, irradiated tmRNA revealed strong stops at U10/C11 and U26/U27/U28/G29 near the 5′ terminus as well as A327/U328/U329/U330, C343, and U347/C348 near the 3′ terminus. To differentiate between photodamaged and cross-linked nucleotides, primer extension analysis was also carried out on tmRNA species that had been irradiated but not cross-linked (Figure 1A). These molecules were expected to carry the same assortment of modifications as XL-tmRNA but lack

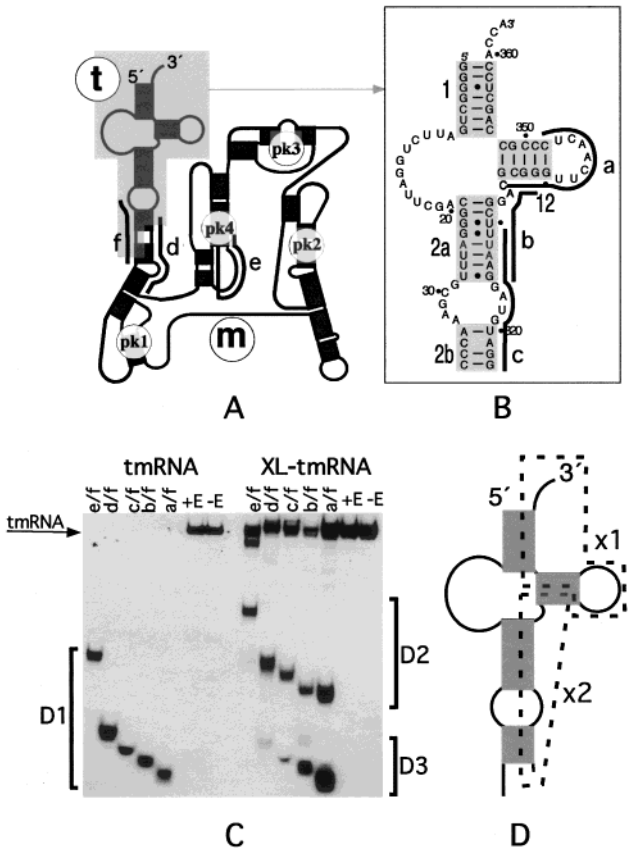

FIGURE 3: Localization of the cross-linked segments in the *E. coli* tmRNA by RNase H analysis. Panels A, B: The sites of hybridization of oligodeoxyribonucleotides a−f (black lines) in tmRNA and its tRNA-like domain. Letters t and m identify tRNA- and mRNA-like domains of tmRNA. Pseudoknots are labeled pk1−pk4. Numbers 1, 2a, 2b, and 12 denote helical segments of the tRNA-like domain. Panel C: Autoradiograms of RNase H digests of 3′-^{32}P-labeled tmRNA (left panel) and XL-tmRNA (right panel) carried out in the presence of a/f, b/f, c/f, d/f, and e/f pairs of oligodeoxyribonucleotides and fractionated on a 10% polyacrylamide gel. Controls: +E, incubation with RNase H in the absence of oligodeoxyribonucleotides; −E, incubation without RNase H or oligodeoxyribonucleotides. D1, D2, and D3 denote series of fragments of tmRNA produced by RNase H digestion of tmRNA and XL-tmRNA. Panel D: Schematic representation of the results of RNase H analysis of XL-tmRNA. x1 and x2 identify two 3′-end sites of cross-linking in tmRNA.

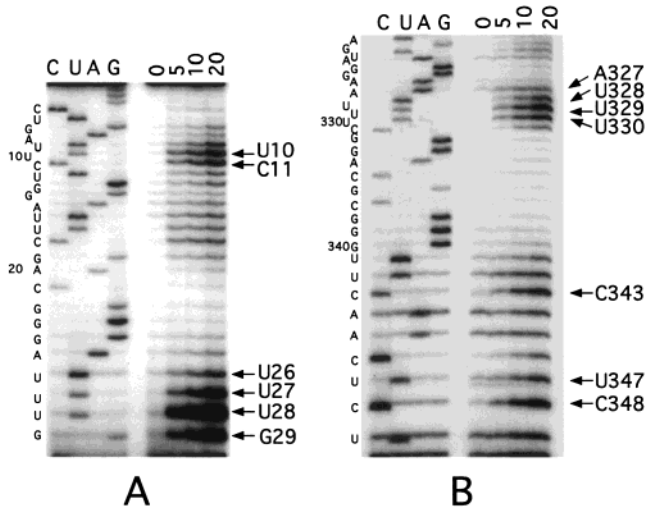

FIGURE 4: Primer extension analysis of cross-linked nucleotides. Panel A: Autoradiogram of the 5′-terminal segment of XL-tmRNA in the presence of oligodeoxyribonucleotide 5′-oligo complementary to nucleotides 53−67. Panel B: Same analysis of the 3′-terminal segment of tmRNA in the presence of the oligodeoxyribonucleotide 3′-oligo complementary to nucleotides 352−363. Sequences of the analyzed segments of tmRNA are indicated on the left side of the autoradiograms. Stop signals corresponding to the nucleotides preceding the cross-link sites are indicated by arrows, and nucleotide symbols and their numbers in the *E. coli* tmRNA are on the right side of the autoradiograms. C, U, A, and G are sequencing lanes. Numbers above lanes refer to minutes of UV irradiation.

the cross-links responsible for XL-tmRNA retardation on denaturing polyacrylamide gels. Uncross-linked tmRNA revealed a strong stop at C343 and weaker signals at U28/G29 (not shown). Therefore, assuming that the arrest occurred at one residue 3′ of the cross-linked nucleotide (*31*), the results indicated that U9/U10, A25/U26/U27/U28, A326/A327/U328/U329, and C346/U347 formed cross-links. In contrast, U342 and a portion of U27/U28 were most likely photodamaged or cross-linked to adjacent uridines on the same RNA strand, as supported by earlier studies, which demonstrated the formation of cyclobutane dimers in RNA (*32*, *33*).

To determine which pairs of nucleotides formed cross-links x1 and x2, a second round of RNase H digestions of the 3′-^{32}P-labeled XL-tmRNA was carried out in the presence of chimeric oligonucleotides h1, h2, or h3, which facilitated precise cutting between residues 13−15, 337−339, or 343−345 (see Figure 5B). RNase H digestion of 3′-^{32}P-labeled XL-tmRNA with oligonucleotide pairs h1/h3 and h2/h3 released short cross-linked complexes consisting of 3′- and 5′-terminal segments of tmRNA (Figure 5A, right panel), thereby identifying U9/U10 and C346/U347 as partners in cross-link x1. Addition of [5′-^{32}P]-pCp and T4 RNA ligase to the same RNase H digests labeled the 3′ end of the cross-linked loop formed by an internal segment of tmRNA encompassing nucleotides 15−338 (not shown). This finding confirmed the presence of cross-link x2, already indicated by RNase H analyses of the 3′-^{32}P-labeled XL-tmRNA (Figures 3C and 5A) and identified A25/U26/U27/U28 and A326/A327/U328/U329 as being cross-linked.

UV Cross-Linking of Truncated tmRNA Derivative. Two-thirds of *E. coli* tmRNA is composed of four pseudoknots (pk1−pk4) (see Figure 3A). Deletion of individual pseudoknots pk2, pk3, or pk4 did not influence tmRNA peptide-tagging functions in vitro (*34*). In contrast, deletion or alteration of pk1 affected both the structure and the function of tmRNA (*35*). A truncated tmRNA, tmRNAΔ90−299, which lacks nucleotides 90−299 (including pk2−pk4), was unable to bind 70S ribosomes but was aminoacylated as efficiently as full-length tmRNA (*7*). Figure 1A shows that irradiation of tmRNAΔ90−299 also yielded a cross-linked product, XL-tmRNAΔ90−299. The kinetics and efficiency of this reaction were similar to those observed in the cross-linking of full-length tmRNA. Moreover, RNase H degradation and primer extension analysis of XL-tmRNAΔ90−299 revealed cross-links identical to those found in XL-tmRNA (not shown). Taken together, these data provide additional evidence that pseudoknots pk2−pk4 have no influence on the proper folding of the tRNA-like domain.

Comparative Sequence Analysis of tmRNA. An alignment of 79 tmRNA sequences was generated to determine variable and conserved features within the tRNA-like domain of tmRNA. Sequences were from all subdivisions of bacteria

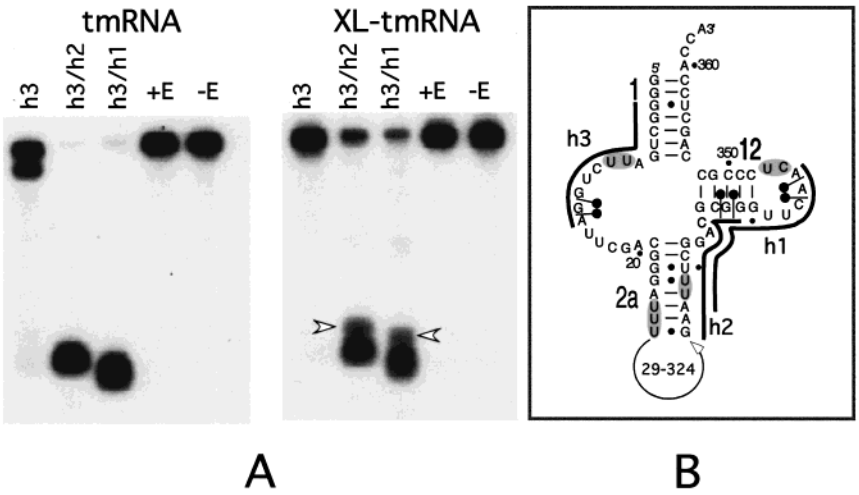

FIGURE 5: Dissection of the tRNA-like domain of the XL-tmRNA by RNase H analysis. Panel A: Autoradiograms of RNase H digests of 3′-^{32}P-labeled tmRNA (left panel) and XL-tmRNA (right panel) carried out in the presence of oligodeoxyribonucleotides h3, h1/h3, and h2/h3 and fractionated on a 10% polyacrylamide gel. Open arrows indicate covalent complexes of 3′- and 5′-terminal fragments of tmRNA. Controls: +E, incubation with RNase H in the absence of oligodeoxyribonucleotides; −E, incubation without RNase H or oligodeoxyribonucleotides. Panel B: The sites of hybridization of chimeric oligonucleotides h1−h3 (black lines) in tRNA-like domain. "Lollipops" indicate cleavages induced by RNase H. Numbers 1, 2a, 2b, and 12 denote helical segments of the tRNA-like domain.

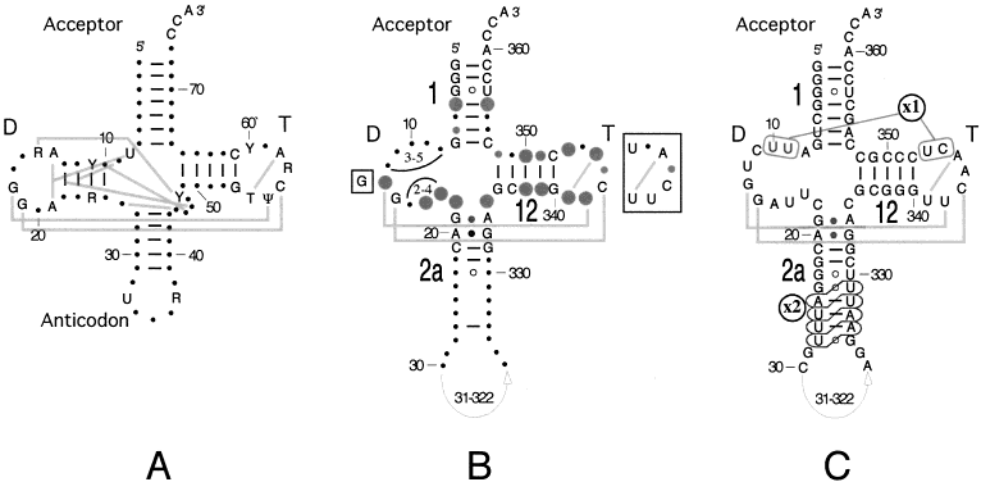

FIGURE 6: Structural features of tRNA and tmRNA. Panel A: Structural domains of the tRNA cloverleaf. Letters indicate conserved residues in the acceptor (AC), D domain (D), anticodon (AN), and T domain (T). R and Y designate purine and pyrimidines, respectively; Ψ is for pseudouridine. Residues are numbered from the 5′ end according to the nomenclature of Sprinzl et al. (*54*). Gray lines indicate nine tertiary interactions (*55*, *56*). Panel B: Consensus secondary structure of the tRNA-like portion of tmRNA derived from the analysis of 79 tmRNA sequences. Numbering of residues and helices 1, 2a, and 12 is according to tmRNA of *E. coli* (*5*). Letters are for invariant residues. Extent of conservation is shown by dot diameters, where large dots mark positions conserved in more than 90% of sequences, medium dots indicate 75% conservation, and small dots show conservation in more than half of known tmRNAs. Base pairs supported by comparative sequence analysis (*5*) are drawn as lines for Watson−Crick pairings, open circles for G-U, or solid dots for G-A interactions. Pairings of invariant residues (which cannot be supported by phylogenetic comparison) are included if present in equivalent positions of conventional tRNA. Incorporated are pairings between invariant 19-GAC-21 and 332-GGA-334. Numbers within the D loop indicate residue ranges. Possible tertiary interactions are indicated by gray lines. Boxed residues indicate sequence conservation in all bacteria but excluding the α-proteobacteria. Modified residues, 5-methyl-U341/U342 and U347 (*57*), are not shown because in vitro-transcribed RNA was used in this study. C: tRNA-like portion of *E. coli* tmRNA with the secondary structure drawn as in Figure 3B. Residues involved in cross-link 1 (x1) and cross-link 2 (x2) are indicated.

as well as several bacteria-related organelle sequences. Duplicate or incomplete tmRNA terminal sequences were excluded from the analysis to produce a representative alignment, which was the basis for the consensus secondary structure shown in Figure 6B. Comparison of this consensus pattern with the canonical tRNA shown in Figure 6A revealed that acceptor and T domains were very similar. The number of base pairs of the helical regions was conserved, as was the U341/A345 interaction within the T loop (equivalent to the T54/A58 pairing in tRNA) and the parallel pairing of 13-GG-15 (tRNA residues 18-GG-19) with two pyrimidines of T loop. This pattern deviated somewhat only in the α-proteobacteria. The D domain of tmRNA was reduced considerably in all bacterial subdivisions. Only 3−5 residues preceded the 13-GG-15 dimer, and 2−4 residues followed the 13-GG-15 dimer. As a result, numerous tertiary interactions involving the D arm of tRNA cannot occur in tmRNA. The variable region that connects the anticodon and T domains of tRNA was also reduced or missing. Features unique to tmRNA were an invariant base pair between C21 and G332 and an extension of this pair by two proposed AG interactions (19-GA-20 with 333-GA-334). Although

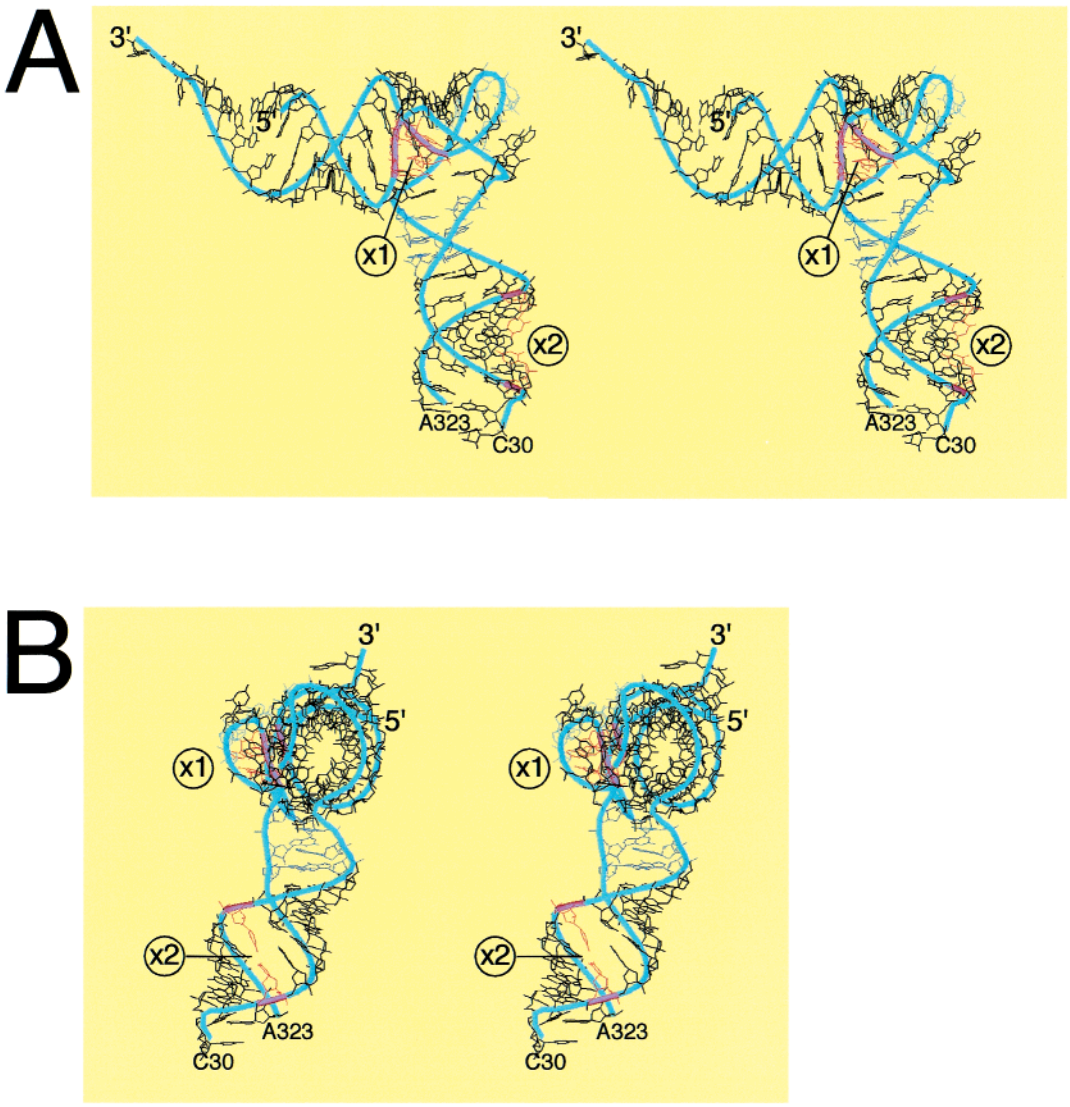

FIGURE 7: Three-dimensional model of the tRNA domain of *E. coli* tmRNA. Panel A: Stereoview showing the RNA backbone as a blue ribbon. Cross-links x1 and x2 are labeled as such and highlighted by purple ribbon sections and residues in red. The interaction between the D and the T domains (13-GG-14 with 342-UC-343) at the corner of the L is drawn in light blue; the structure of 18-CGA-20 with 333-GAC-335 is in dark blue. The 3′ and 5′ ends are labeled as such. Numbering is according to *E. coli* tmRNA (see also Figure 3B). The model and figure were generated with RNA modeling program ERNA-3D (*24*) on a Silicon Graphics Octane workstation. Panel B: Stereoview of the model shown in A, turned by 90°, with the tmRNA ends pointing away from the viewer.

present in the crystal structures of the RNA hammerhead ribozyme (*27*) and a region of 23S rRNA of *Haloarcula marismortui* (*26*), these pairings could not be confirmed due to the limitations of comparative sequence analysis.

tmRNA Modeling. Using ERNA-3D software (*24*), the secondary structural features described above were incorporated into the three-dimensional model for the tRNA-like domain of *E. coli* tmRNA shown in Figure 7. Modeling was initiated by assuming A-form RNA conformations for helices 1, 2a, and 12 (see Figure 6B,C). Helices 1 and 12 were adjusted manually in an approximate coaxial configuration with yeast $tRNA^{Phe}$ as a template. Backbone conformation of the T loop and the reverse Hoogsteen GG-T interaction between the D and T loops were transferred from the crystal structure of yeast $tRNA^{Phe}$ to fix this conserved tertiary interaction in three dimensions. Similarly, backbone coordinates of the two imino type G·A base pairs and the flanking Watson−Crick U-A were extracted from the RNA hammerhead 28-mer (*27*) and superimposed onto 18-CGA-20 and 332-GAC-335. The adjacent C18 and C335 were placed in a base pair-like manner. Justification for this configuration was weak by comparative analysis, as these two C residues are highly conserved. However, compatible A-U and A-C changes are observed in MYC.GEN., MYC.PNE., and URE.URE. (Species abbreviations are those used in tmRDB; *22*.) With a similar degree of justification, A8 and U17 were placed as approximate Watson−Crick pairs. This placement may be comparable to the interaction proposed in mitochondrial type II tRNA-Ser DS5081 from *Strongylocentrotus purpuratus* (*36*). For two short regions, 9-UUCU-12 and 15-AUU-17, there was no structural information available. These regions, therefore, were modeled using the chain-translocation algorithm offered by ERNA-3D. The possible G3-U73 wobble base pair of the acceptor stem (*10*), an identity element in $tRNA^{Ala}$ (*37*−*39*), was not included.

Cross-linked residues 9-UU-10 and 346-CU-347 were brought into close proximity and rotated into coplanar configurations at distances of <5 Å to be compatible with the relative geometries of cyclobutane dimers (*12*, *32*, *40*). A slight imperfection was introduced into helix 2a to

accommodate cross-link x2. The model was refined using VCMD software (*28*) to bond deviations of <0.20 Å (Figure 7). PDB coordinates of the model are available from the tmRDB at the Internet address psyche.uthct.edu/dbs/tmRDB/.

DISCUSSION

Comparing sequences of the *E. coli* ssrA gene (*41*), Komine et al. (*8*) first noticed that the 3′- and 5′-terminal segments of tmRNA could be arranged into a structure that resembled the acceptor and T arms of canonical cytoplasmic tRNAs. They also demonstrated that, as in tRNA, the 5′ end of tmRNA is generated by RNase P, and mature tmRNA can be aminoacylated with alanine. The notion that terminal segments of tmRNA resemble tRNA was strengthened further by observations that the 3′ CCA terminus is repaired by ATP/CTP tRNA nucleotidyl transferase (*7*) and that tmRNA interacts with ribosomes (*9*−*10*) and facilitates peptide tagging (*6*). Comparative analyses of available sequences and chemical probing (*3*−*5*) revealed a tRNA-like domain connected to a mRNA-like domain by one or more pseudoknots (*3*, *42*).

While extensive functional homologies between tRNA and tmRNA are supported by compelling experimental data (*43*−*46*), there is only partial structural similarity between the tRNA and the tRNA-like domain of tmRNA. Unlike the acceptor and T arms, the D domains of tmRNA and tRNA are substantially different. In tmRNA, the D domain is reduced to 10−13 nucleotides, which cannot form an equivalent of the D stem with 3−4 base pairs. Because six of the nine long-range interactions that stabilize tRNA are not provided by the D domain of tmRNA, it is possible that this molecule might not be able to mimic completely the three-dimensional folding of canonical tRNA molecules (*2*). In addition, the section of tmRNA containing helix 2a bears no discernible similarity to the anticodon arm of tRNA. Also, because tmRNAΔ90−299 is unable to bind to 30S ribosomal subunits that lack protein S1 (*7*), it seems unlikely that any part of helix 2 constitutes a functional or structural homologue of the anticodon arm, which in tRNA contributes the main part of free energy of binding to 70S ribosomes (*47*, *48*).

To determine whether similarities between the canonical tRNA and the tRNA-like domain of tmRNA extend beyond acceptor and T arms, we applied a cross-linking approach that relies on direct photolysis of unmodified RNA with far-UV light. Because cross-linking generates covalent bonds with a length of 3−5 Å, only nucleotides that are in close proximity can participate in the reaction. Our studies showed that unmodified *E. coli* tmRNA, when irradiated with 254 nm of light, formed two main intramolecular cross-links. Cross-link x1 involved nucleotides U9/U10 and C346/U347, while cross-link x2 joined nucleotides U26/U27/U28 and U328/U329, thus proving that these residues, although far apart in the sequence, are close in three dimensions. Because the cross-links did not reduce the charging capacity of tmRNA and were formed with ribosome-bound tmRNA, this spatial arrangement must reflect a functional conformation of tmRNA both on and off the ribosome. Pseudoknots pk2−pk4 do not greatly affect the folding of the 3′- and 5′-terminal segments of tmRNA, since the same cross-links were formed in tmRNAΔ90−299. This suggestion is supported by earlier studies, which showed that deletion of pk2, pk3, or pk4 does not affect the peptide-tagging function of tmRNA (*34*). Cross-link x1 between U9/U10 and C346/U347 demonstrates the close proximity of the D domain and T loop. Because it is reversed by additional UV irradiation, is not fluorescent, and resists treatment with diluted HCl, x1 probably belongs to the cyclobutane dimer class (*32*, *49*, *50*). Therefore, the 5−6 double bonds of the pyrimidine rings in the U9/U10 and C346/U347 residues must be able to rotate into a nearly parallel configuration approximately 5 Å apart (*33*). Such an arrangement is adopted by C48 and U59 in UV treated cross-linked unmodified yeast $tRNA^{Phe}$ (*12*). Because A9/G10 and U59/C60 (the equivalents of U9/U10 and C346/U347) are far apart in the elbow region of the L-shaped structure of yeast $tRNA^{Phe}$, cross-link x1 highlights a structural detail that is significantly different.

The cross-link x2 between residues at positions 25−28 and 326−329 is, in general, consistent with a helical structure of tmRNA helix 2a (*3*−*5*). Although we do not know which of the five U residues formed covalently bound pairs, incorporation of U26 and U328 in a configuration resembling the cyclobutane pyrimidine dimer introduced the smallest distortion in this region (Figure 7B), which does not preclude formation of cross-links between A25 and U329, U27 and A327, and U28 and A326. Imperfections in helix 2a of numerous tmRNAs are indicated also by comparative sequence analysis (*22*). Furthermore, Felden et al. (*4*) observed an unusual probing pattern between nucleotides A8 and U33, suggesting that the 2a region may breathe considerably.

The alignment of 79 representative tmRNA sequences provided the basis for the consensus secondary structure of the tRNA-like domain of tmRNA (Figure 6B) and demonstrated that only three out of the nine long-range interactions that contribute to the L-shape folding of canonical tRNA are likely to be present in tmRNA (Figure 6A). This suggestion is consistent with the comparative sequence analysis of the mitochondrial tRNAs, which showed that, despite missing parts of D and/or T arms, these tRNAs seem to adopt the L-shape architecture (*51*).

In contrast to earlier analyses carried out on a small number of tmRNA sequences, the present study does not support base pairing between U9/U10 and G19/A20 residues (analogous to base pairing between 10/11 and 24/25 residues in yeast $tRNA^{Phe}$). It seems more probable that G19/A20 form non-Watson−Crick base pairs with G333/A334. We emphasize that inclusion of these two AG interactions cannot be confirmed by comparative sequence analysis because of their invariant nature (Figures 6B,C and 7). However, similar configurations have been observed in two unrelated RNA molecules and thus present themselves as structural motifs. Furthermore, structural constraints involving the two invariant AGs and possibly coordinated magnesium ions are the most likely explanation for their conservation. Also, it should be noted that the flanking 21-CG-332 pair is invariant, a feature not found in canonical tRNAs. Modular replacement of the RNA hammerhead's imino G-As with a similar structure involving sheared G-As in 23S rRNA (positions 795 and 818) did not alter the model significantly, changing the cross phosphate−phosphate distance only by 1.13 Å. It is unclear, however, which of the two possibilities, or a combination thereof, might exist in tmRNA.

Despite reduction of the D domain and many missing tertiary interactions, overall, the tmRNA structure shown in Figure 7 is remarkably similar to that of canonical tRNA. This is in agreement with the ability of tRNA-specific enzymes to process, modify, and charge tmRNA (*7*, *44*, *45*). In contrast to canonical tRNAs, some unknown degree of flexibility seems to be maintained between the two arms of tmRNA molecules. For magnesium ion concentrations of 10−15 mM, the interstem angle for tmRNA is approximately 10° larger than the corresponding angle for yeast $tRNA^{Phe}$ in solution (∼90°; *52*). Recent transient electric birefringence measurements indicate that the tRNA-like domain resembles a "boomerang", with an interstem angle of 110° (*53*). It remains to be investigated to what extent increased flexibility, unusual folding in the elbow region, and a relaxed conformation in helix 2a might play a role in tmRNA function. The three-dimensional model of the tRNA-like domain of tmRNA presented here is expected to facilitate these efforts.

ACKNOWLEDGMENT

We thank Florian Müller for a more powerful version of ERNA-3D and generous advice. We are grateful to Ingolf Sommer for providing VCMD refinement software.

REFERENCES

1. Karzai, A. W., Roche, E. D., and Sauer, R. T. (2000) *Nat. Struct. Biol. 7*, 449−455.
2. Wower, J., Zwieb, C., and Wower, I. K. (2000) in *The Ribosome*: *Structure*, *Function*, *Antibiotics*, *and Cellular Interactions* (Garrett, R. A., Douthwaite, S. R., Liljas, A., Matheson, A. T., Moore, P. B., and Noller, H. F., Eds.) pp 397−405, ASM Press, Washington, DC.
3. Williams, K. P., and Bartel, D. P. (1996) *RNA 2*, 1306−1310.
4. Felden, B., Himeno, H., Muto, A., McCutcheon, J. P., Atkins, J. F., and Gesteland, R. F. (1997) *RNA 3*, 89−103.
5. Zwieb, C., Wower, I. K., and Wower, J. (1999) *Nucleic Acids Res. 27*, 2063−2071.
6. Keiler, K. C., Waller, P. R., and Sauer, R. T. (1996) *Science 271*, 990−993.
7. Wower, I. K., Zwieb, C. W., Guven, S. A., and Wower, J. (2000) *EMBO J. 19*, 6612−6621.
8. Komine, Y., Kitabatake, M., Yokogawa, T., Nishikawa, K., and Inokuchi, H. (1994) *Proc. Natl. Acad. Sci. U.S.A. 91*, 9223−9227.
9. Ushida, C., Himeno, H., Watanabe, T., and Muto, A. (1994) *Nucleic Acids Res. 22*, 3392−3396.
10. Tadaki, T., Fukushima, M., Ushida, C., Himeno, H., and Muto, A. (1996) *FEBS Lett. 399*, 223−226.
11. Karzai, A. W., Susskind, M. M., and Sauer, R. T. (1999) *EMBO J. 18*, 3793−3799.
12. Behlen, L. S., Sampson, J. R., and Uhlenbeck, O. C. (1992) *Nucleic Acids Res. 20*, 4055−4059.
13. Downs, W. D., and Cech, T. R. (1990) *Biochemistry 29*, 5605−5613.
14. Brimacombe, R., Greuer, B., Gulle, H., Kosack, M., Mitchell, P., Osswald, M., Stade, K., and Stiege, W. (1990) in *The Ribosome* (Hill, W. E., Dahlberg, A., Garrett, R. A., Moore, P. B., Schlessinger, D., and Warner, J. R., Eds.) pp 93−106, ASM Press, Washington, DC.
15. Sternbach, H., von der Haar, F., Schlimme, E., Gaertner, E., and Cramer, F. (1971) *Eur. J. Biochem. 22*, 166−172.
16. Sampson, J. R., and Uhlenbeck, O. C. (1988) *Proc. Natl. Acad. Sci. U.S.A. 85*, 1033−1037.
17. Varshney U., Lee, C. P., and RajBhandary, U. L. (1991) *J. Biol. Chem. 266*, 24712−24718.
18. Wower, J., Hixson, S. S., and Zimmermann, R. A. (1988) *Biochemistry 27*, 8114−8121.
19. Brimacombe, R., Greuer, B., Gulle, H., Kosack, M., Mitchell, P., Osswald, M., Stade, K., and Stiege, W. (1990) in *Ribosomes and Protein Synthesis. A Practical Approach* (Spedding, G., Ed.) pp 131−159, Oxford University Press, Oxford, U.K.
20. Döring, T., Mitchell, P., Osswald, M., Bochkariov, D., and Brimacombe, R. (1994) *EMBO J. 13*, 2677−2685.
21. Baranov, P. V., Dokudovskaya, S. S., Oretskaya, T. S., Dontsova, O. A., Bogdanov, A. A., and Brimacombe, R. (1997) *Nucleic Acids Res. 25*, 2266−2273.
22. Knudsen, B., Wower, J., Zwieb, C., and Gorodkin, J. (2001) *Nucleic Acids Res. 29*, 171−172.
23. Larsen, N., and Zwieb, C. (1991) *Nucleic Acids Res. 19*, 209−215.
24. Müller, F., Doring, T., Erdemir, T., Greuer, B., Junke, N., Osswald, M., Rinke-Appel, J., Stade, K., Thamm, S., and Brimacombe, R. (1995) *Biochem. Cell. Biol. 73*, 767−773.
25. Sussman, J. L., Holbrook, S. R., Warrant, R. W., Church, G. M., and Kim, S.-H. (1978) *J. Mol. Biol. 123*, 607−630.
26. Ban, N., Nissen, P., Hansen, J., Moore, P. B., and Steitz, T. A. (2000) *Science 289*, 905−920.
27. Scott, W. G., Murray, J. B., Arnold, J. R. P., Stoddard, B. L., and Klug, A. (1996) *Science 274*, 2065−2069.
28. Sommer, I., and Brimacombe, R. (2001) *J. Comput. Chem.*, in press.
29. Hagenbuchle, O., Santer, M., Steiz, J. A., and Mans, R. J. (1978) *Cell 13*, 551−563.
30. Barta, A., Steiner, G., Brosius, J., Noller, H. F., and Kuechler, E. (1984) *Proc. Natl. Acad. Sci. U.S.A. 81*, 3607−3611.
31. Denman, R., Colgan, J., Nurse, K., and Ofengand, J. (1988) *Nucleic Acids Res. 16*, 165−178.
32. Kochetkov, N. K., and Budovskii, E. I., Eds. (1972) *Organic Chemistry of Nucleic Acids* Part B, Chapter 12, p 42, Plenum, New York.
33. Patrick, M. H., and Rahn, R. O. (1976) in *Photochemistry and Photobiology of Nucleic Acids* (Wang, S. Y., Ed.) Vol. II, pp 35−95, Academic Press, New York.
34. Nameki, N., Tadaki, T., Himeno, H., and Muto, A. (2000) *FEBS Lett. 470*, 345−349.
35. Nameki, N., Felden, B., Atkins, J. F., Gesteland, R. F., Himeno, H., and Muto, A. (1999) *J. Mol. Biol. 286*, 733−744.
36. Steinberg, S., Gautheret, D., and Cedergren, R. (1994) *J. Mol. Biol. 236*, 982−989.
37. Hou, Y. M., and Schimmel, P. (1988) *Nature 333*, 140−145.
38. McClain, W. H., and Foss, K. (1988) *Science 240*, 793−6.
39. Mueller, U., Schubel, H., Sprinzl, M., and Heinemann, U. (1999) *RNA 5*, 670−677.
40. Ofengand, J., and Liou, R. (1980) *Biochemistry 21*, 4814−4822.
41. Chauhan, A. K., and Apirion, D. (1989) *Mol. Microbiol. 3*, 1481−1485.
42. Zwieb, C., Müller, F., and Wower, J. (1999) *Nucleic Acids Symp. Ser.* No. *41*, 200−204.
43. Tu, G. F., Reid, G. E., Zhang, J.-G., Moritz, R. L., and Simpson, R. J. (1995) *J. Biol. Chem. 270*, 9322−9326.
44. Li, Z., Pandit, S., and Deutscher, M. P. (1998) *Proc. Natl. Acad. Sci. U.S.A. 95*, 2856−2861.
45. Nameki, N., Tadaki, T., Muto, A., and Himeno, H. (1999) *J. Mol. Biol. 289*, 1−7.
46. Barends, S., Wower, J., and Kraal, B. (2000) *Biochemistry 39*, 2652−2658.
47. Rose, S. J., Lowary, P. T., and Uhlenbeck, O. (1983) *J. Mol. Biol. 167*, 103−117.
48. Nekhai, S. A., Parfenov, D. V., and Saminsky, E. M. (1994) *Biochim. Biophys. Acta 1218*, 481−484.
49. Favre, A., and Yaniv, M. (1971) *FEBS Lett. 17*, 236−241.
50. Hauswirth, W., and Wang, S. Y. (1973) *Biochem. Biophys. Res. Commun. 51*, 819−826.
51. Helm, M., Brule, H., Friede, D., Giege, R., Putz, D., and Florentz, C. (2000) *RNA 6*, 1356−1379.
52. Friederich, M. W., Gast, F. U., Vacano, E., and Hagerman, P. J. (1995) *Proc. Natl. Acad. Sci. U.S.A. 92*, 4803−4807.

53. Stagg, S. M., Frazer-Abel, A. A., Hagerman, P. J., and Harvey, S. C. (2000) *Second Symposium on Structural Aspects of Protein Synthesis*, p 63, Rensselaerville, NY.
54. Sprinzl, M., Horn, C., Brown, M., Ioudovitch, A., and Steinberg, S. (1998) *Nucleic Acids Res. 26*, 148−153.
55. Jack, A., Ladner, J. E., and Klug, A. (1976) *J. Mol. Biol. 108*, 619−649.
56. Sussman, J. L., and Kim, S.-H. (1976) *Science 192*, 853−858.
57. Felden, B., Hanawa, K., Atkins, J. F., Himeno, H., Muto, A., Gesteland, R. F., McCloskey, J. A., and Crain, P. F. (1998) *EMBO J. 17*, 3188−3196.

BI010443V